Proc. Natl. Acad. Sci. USA
Vol. 85, pp. 1844–1848, March 1988
Biophysics

Class I major histocompatibility complex proteins diffuse isotropically on immune interferon-activated endothelial cells despite anisotropic cell shape and cytoskeletal organization: Application of fluorescence photobleaching recovery with an elliptical beam

(lateral mobility/actin cytoskeleton/stress fibers/fluorescein phosphatidylethanolamine)

ALAN H. STOLPEN†, JORDAN S. POBER‡, CARL S. BROWN†, AND DAVID E. GOLAN†§¶

†Department of Biological Chemistry and Molecular Pharmacology, Harvard Medical School, and Departments of ‡Pathology and §Medicine (Hematology Division), Brigham and Women's Hospital and Harvard Medical School, Boston, MA 02115

Communicated by Elkan Blout, December 4, 1987

ABSTRACT Interferon γ induces striking phenotypic alterations in confluent cultures of human vascular endothelial cells (HEC), including cell shape change from polygonal to elongated and cytoskeletal actin rearrangement from dense peripheral bands to longitudinal bundles of stress fibers. Since many transmembrane proteins, including class I major histocompatibility complex (MHC) proteins, interact with cytoskeletal actin, an interferon-γ-induced anisotropic arrangement of stress fibers might cause anisotropic lateral diffusion of HEC class I MHC proteins. To test this hypothesis, we adapted the fluorescence photobleaching recovery technique to allow measurement of anisotropic diffusion of fluorescently labeled molecules on two-dimensional surfaces. A highly eccentric elliptical Gaussian laser beam was used to photobleach the sample and to monitor fluorescence recovery. In this technique, named "line fluorescence photobleaching recovery," lateral diffusion is measured along that axis of the sample that is perpendicular to the major axis of the elliptical beam. The lateral diffusion coefficient and fractional mobility are obtained by fitting the experimental data to a theoretical recovery curve, the form of which is determined by the solution to a modified version of the diffusion equation in which a tensor is used to describe diffusion in two orthogonal directions. Fluorescein-conjugated murine monoclonal antibodies were used to label class I MHC proteins on interferon-γ-treated HEC and human dermal fibroblasts. These two cultured human cell types were found to be similar in their elongated shape and anisotropic stress fiber organization. Class I MHC protein lateral mobility was compared to that of fluorescein-labeled phosphatidylethanolamine, a membrane phospholipid probe. Class I MHC proteins diffused anisotropically on human dermal fibroblasts, whereas fluorescein-labeled phosphatidylethanolamine diffused isotropically on this cell type. In contrast, both class I MHC proteins and fluorescein-labeled phosphatidylethanolamine diffused isotropically on interferon-γ-treated HEC. These data suggest that neither elongated shape nor anisotropic stress fiber arrangement is sufficient to induce anisotropic diffusion of proteins on the HEC plasma membrane.

The plasma membranes of vascular endothelial cells form the interface between the blood and the underlying vessel wall and tissues. Interactions between the endothelial cell surface and blood cells or macromolecules may depend not only on the detailed molecular composition and organization of the membrane but also on the dynamic motion of specific cell surface components. Immunological and inflammatory mediators have been shown to alter the phenotype of cultured endothelial cells. After treatment with immune interferon [interferon γ (IFN-γ)], for example, the expression of class I and class II major histocompatibility complex (MHC) antigens is increased (1), cell shape is changed from polygonal to elongated, cytoskeletal actin is rearranged from dense peripheral bands to longitudinal arrays of stress fibers (SF), and the extracellular fibronectin matrix is degraded (2). The effects of IFN-γ on the lateral mobility of specifically labeled surface molecules have not been examined previously.

Since the lateral diffusion of plasma membrane proteins is often much slower than that of membrane lipid (3–5), it has been hypothesized that interactions with the cytoskeleton restrict membrane protein mobility (6–13). Anisotropic cytoskeletal arrangements might, therefore, cause membrane proteins to diffuse anisotropically. Smith *et al.* (14) showed that con A receptors on murine fibroblasts diffuse anisotropically, such that the direction of fastest diffusion is parallel to the underlying actin SF. In contrast, Kapitza *et al.* (15) found that con A receptor diffusion on human foreskin fibroblasts is isotropic.

We have developed a theory and adapted an experimental method for measuring anisotropic lateral diffusion on cell surfaces. The method is based on fluorescence photobleaching recovery (FPR), a technique for measuring lateral diffusion of fluorescently labeled cell surface molecules (16, 17). In our "line FPR" technique, a pair of cylindrical lenses is used to transform the cross-sectional profile of the excitation laser beam from a circular to an elliptical Gaussian profile (see also ref. 18). Because recovery kinetics in line FPR experiments are dominated by lateral diffusion perpendicular to the major axis of the elliptical beam, the technique can be used to measure diffusion in a single direction. We have applied this method to quantify the diffusion, in two orthogonal directions, of class I MHC proteins and of membrane phospholipid on IFN-γ-treated human endothelial cells (HEC), and compared these results with those obtained on human dermal fibroblasts (HDF). Despite the observation that both of these cell types manifest elongated shape and anisotropic SF organization, HDF, but not HEC, exhibit anisotropic diffusion of class I MHC proteins.

The publication costs of this article were defrayed in part by page charge payment. This article must therefore be hereby marked "*advertisement*" in accordance with 18 U.S.C. §1734 solely to indicate this fact.

Abbreviations: Flu-PtdEtn, fluorescein-labeled phosphatidylethanolamine; FPR, fluorescence photobleaching recovery; HDF, human dermal fibroblasts; HEC, human endothelial cells; IFN-γ, immune interferon or interferon γ; MHC, major histocompatibility complex; SF, stress fibers; β_2m, β_2-microglobulin.

¶To whom reprint requests should be addressed.

THEORY

Anisotropic diffusion on a two-dimensional surface is modeled by a version of the diffusion equation in which the scalar diffusion coefficient, D, is replaced by the constant tensor $\mathbf{D}$ (see refs. 14 and 19):

$$\partial C(x, y, t)/\partial t = -\nabla \cdot \mathbf{D} \cdot \nabla^{\mathrm{T}} C(x, y, t), \quad [1]$$

where ∇ is the gradient operator $(\partial/\partial x, \partial/\partial y)$, ∇^{T} is the transpose of ∇, and $C(x, y, t)$ is the concentration of unbleached, mobile fluorophore at position (x, y) and time t. Eq. **1** is solved for $C(x, y, t)$ by the method of Fourier transforms (adapted from refs. 14 and 16). The result is valid for all initial conditions:

$$C(x, y, t) = (2\pi M t)^{-1} C(x, y, 0) * \exp\{-[x^2 D_{yy} + y^2 D_{xx} - xy(D_{xy} + D_{yx})]/(M^2 t)\}, \quad [2]$$

where $M = [4D_{xx}D_{yy} - (D_{xy} + D_{yx})^2]^{1/2}$, $C(x, y, 0)$ is the concentration profile immediately after photobleaching, and $*$ is the convolution operator. The form of $C(x, y, 0)$ is determined by the intensity profile of the laser beam and the duration of photobleaching. The beam used in line FPR experiments has an elliptical Gaussian profile, $I(x, y)$:

$$I(x, y) = [2P_0/(\pi w_x w_y)]\exp[-2(x^2/w_x^2 + y^2/w_y^2)], \quad [3]$$

where w_x and w_y are the $1/e^2$ (Gaussian) radii along the minor and major axes of the ellipse, respectively, and P_0 is the laser power. The attenuated beam used to monitor fluorescence recovery has the same intensity profile as the bleaching beam. We define the coordinate (x, y) such that $(0, 0)$ is located at the center of the elliptical beam and the y axis is parallel to the major axis of the ellipse. If it is assumed that photobleaching is a first-order process, then:

$$C(x, y, 0) = C_0 \exp[-KI(x, y)/I(0, 0)], \quad [4]$$

where C_0 is the uniform fluorophore concentration before photobleaching and K describes the extent of photobleaching (16). Fluorescence intensity, $F(t)$, is related to $C(x, y, t)$ as follows:

$$F(t) = (q/A) \int_{-\infty}^{\infty} \int_{-\infty}^{\infty} I(x, y)\, C(x, y, t)\, dx\, dy, \quad [5]$$

where q is the product of all quantum efficiencies of absorption, emission, and detection and A is the attenuation factor for the measuring beam.

We solve for $F(t)$ by substituting Eqs. **2–4** in Eq. **5** and then expanding $C(x, y, 0)$ in terms of $KI(x, y)/I(0, 0)$:

$$F(t) = F(\infty) \sum_{n=0}^{\infty} [(-K)^n/n!] \cdot [(1 + n + 2nt/\tau_{xx})(1 + n + 2nt/\tau_{yy}) - (nt/\tau_{xy})^2]^{-1/2}, \quad [6a]$$

where:

$$\tau_{xx} = w_x^2/4D_{xx}, \quad [7a]$$

$$\tau_{yy} = w_y^2/4D_{yy}, \quad [7b]$$

$$\tau_{xy} = w_x w_y/4(D_{xy} + D_{yx}), \quad [7c]$$

and $F(\infty)$ is the fluorescence intensity at infinite time. K satisfies the relation:

$$F(0)/F(\infty) = K^{-1}[1 - \exp(-K)], \quad [8]$$

where $F(0)$ is the fluorescence intensity immediately after photobleaching (cf. equation 7 in ref. 16).

In the limit $\tau_{yy}, \tau_{xy} >> \tau_{xx}$, only τ_{xx} contributes significantly to the terms in Eq. **6a**, and $F(t)$ is well-approximated by:

$$F(t) = F(\infty) \sum_{n=0}^{\infty} [(-K)^n/n!](1 + n + 2nt/\tau_{xx})^{-1/2}. \quad [6b]$$

Since Eq. **6b** represents the limit of Eq. **6a** as the eccentricity of the elliptical beam approaches unity (assuming $D_{xx} > 0$), we call it the "line approximation." Line FPR data are fit to Eq. **6b** (see below). $F(t)$ can be evaluated rapidly and to a high degree of precision because the series converges rapidly. For $K = 10$ (a very large value), $F(t)$ is evaluated to within a 0.01% error by summing the first 31 terms. If only the first two terms of Eq. **6b** are used (valid for $K << 1$), an expression for $F(t)$ is obtained that is similar to that of Koppel (see equations 9 and 12 in ref. 18).

When diffusion is isotropic and the laser beam has a circular Gaussian profile, Eq. **6a** reduces to the solution of the diffusion equation described by Axelrod *et al.* (see equation 12 in ref. 16):

$$F(t) = F(\infty) \sum_{n=0}^{\infty} [(-K)^n/n!](1 + n + 2nt/\tau)^{-1}. \quad [6c]$$

This solution also holds when $\tau_{xx} = \tau_{yy}$ and $\tau_{xy} = \infty$, although diffusion need not be isotropic under these conditions.

EXPERIMENTAL METHODS

Cell Culture. HDF were obtained by explant outgrowth and were serially subcultured. HEC were cultured from umbilical vein as described (20, 21) and used in first passage. All cultures were plated on glass coverslips (precoated with fibronectin at 10 μg/cm^2 for HEC) and treated at subconfluence with recombinant IFN-γ [a gift of Walter Fiers, State University of Ghent, Belgium (22)] as indicated.

Labeling. Cell surface class I MHC proteins were labeled with either fluorescein-conjugated murine monoclonal IgG_1 antibody directed against human β_2-microglobulin (anti-β_2m; Becton Dickinson) or with an IgG_{2a} antibody directed against a monomorphic determinant of HLA-A,B,C (W6/32; see ref. 23), conjugated to fluorescein isothiocyanate as described (24). Alternatively, plasma membranes were labeled with the lipid probe fluorescein-labeled phosphatidylethanolamine (Flu-PtdEtn; Avanti Polar Lipids). A solution of Flu-PtdEtn at 1 mg/ml in chloroform was dried in a rotary evaporator, brought to a final concentration of 5 μg/ml in Medium 199, Vortex mixed, and sonicated until clear. HDF or HEC were incubated with this Flu-PtdEtn solution for 45–50 min at 35°C. Coverslips were mounted in a Sykes–Moore chamber (Bellco Glass) with ≈1 ml of growth medium preequilibrated with 95% air/5% CO_2.

FPR Apparatus. Our spot FPR apparatus is described in ref. 25. This apparatus was modified for line FPR by a pair of planoconvex cylindrical lenses (focal lengths, 25 and 150 cm). These lenses were positioned 175 cm apart, with their optical axes parallel, in the excitation light path.

FPR Measurements. Spot FPR was performed as described (25). For line FPR, the elliptical laser beam was focused on a small, uniformly fluorescent patch of membrane. A rotating microscope stage was used to orient the major axis of the beam either parallel or perpendicular to SF in HDF and HEC. After the prebleach fluorescence intensity was recorded, the laser power was increased briefly to produce the photobleaching pulse. Fluorescence intensity after bleaching was monitored periodically by using the laser at its original power. Recovery of fluorescence was due to lateral diffusion of unbleached fluorophores into the bleached area.

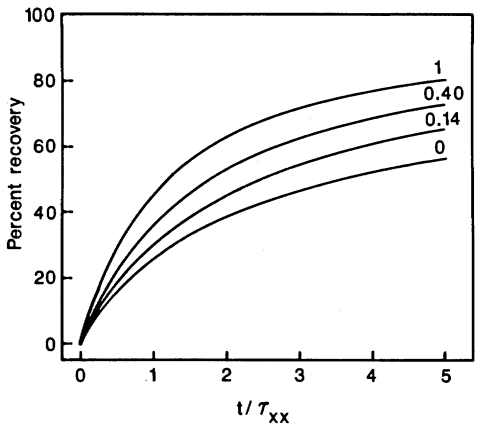

FIG. 1. Effect of τ_{xx}/τ_{yy} ratio on recovery kinetics. Eq. **6a** was evaluated for $K = 2$ (a typical value) at ratios of τ_{xx}/τ_{yy} between 0 and 1. The τ_{xx}/τ_{yy} ratio is indicated above each recovery curve. The ordinate, percent recovery, is given by: $100\cdot[F(t) - F(0)]/[F(\infty) - F(0)]$. The abscissa represents time after photobleaching. For $w_x = w_y$, the top curve represents isotropic diffusion, and the bottom curve represents one-dimensional diffusion.

Cells were maintained at 37°C during all FPR experiments.

Beam Calibration. A two-dimensional scan of the emission diaphragm was used to determine the dimensions of the laser beam at the sample plane (unpublished data). w_x and w_y were determined by a nonlinear least squares fit (26) of the scan data to a version of Eq. **3** that was modified to allow for translational and rotational offsets of the elliptical beam relative to the x and y axes of the mirror scanner. Typical values for w_x and w_y, respectively, were 1.1 and 9.9 μm for protein diffusion measurements and 2.5 and 12.9 μm for lipid diffusion measurements.

Data Analysis. Line FPR data were computer-fit to Eq. **6b** by the nonlinear least squares algorithm of Marquardt (26). $F(t)$ (Eq. **6b**) was evaluated to within a 0.01% error. The diffusion coefficient (D_{xx}) and mobile fraction (f) of fluorophores were calculated from the best-fit values of τ_{xx}, K, and $F(\infty)$ by using Eqs. **7a** and **8** and the expression:

$$f = 100\cdot[F(\infty) - F(0)]/[F(-) - F(0)], \qquad [9]$$

where $F(-)$ is the prebleach fluorescence intensity. Data sets were analyzed in <1 min.

For each biological sample the statistical significance of the difference between the coefficients of diffusion parallel ($D_{\parallel}$) and perpendicular ($D_{\perp}$) to the orientation of actin SF was determined by using the two-tailed Student's t test.

RESULTS

Solution to the Diffusion Equation. The behavior of Eq. **6a** is depicted graphically in Figs. 1 and 2. Fluorescence recovery kinetics are shown for ratios of τ_{xx}/τ_{yy} between 0 and 1 (Fig. 1). Recovery is fastest when $\tau_{xx} = \tau_{yy}$ (Fig. 1, top curve) and slowest when $\tau_{yy} >> \tau_{xx}$ (Fig. 1, bottom curve). Recovery half-times, $\tau_{1/2}$, defined by:

$$[F(\tau_{1/2}) - F(0)]/[F(\infty) - F(0)] = 0.5, \qquad [10]$$

increase ≈3-fold from $\tau_{xx}/\tau_{yy} = 1$ to $\tau_{xx}/\tau_{yy} = 0$.

When a sample that exhibits diffusion anisotropy is rotated with respect to the elliptical beam, fluorescence recovery kinetics are altered (Fig. 2*A*). Rotation through the angle θ is equivalent to transformation of the diffusion tensor as follows:

$$\mathbf{D}(\theta) = \mathbf{R}(\theta)\cdot\mathbf{D}\cdot\mathbf{R}^{-1}(\theta), \qquad [11]$$

where $\mathbf{R}(\theta)$ is the unitary rotational transformation matrix. (For $w_x = w_y$ Eq. **6a** is independent of θ, implying that spot FPR measurements are unaffected by sample orientation.) If the principal axes of diffusion are parallel to the major and minor axes of the elliptical beam, then **D** is represented by a diagonal matrix. Under this condition $D_{xx}(\theta)$ is described by:

$$D_{xx}(\theta) = D_{xx}\cos^2\theta + D_{yy}\sin^2\theta \qquad [12]$$

(see also ref. 14). Further, if the major axis of the elliptical beam is parallel to the y axis, then $D_{xx}(\theta)$ represents the diffusion rate in the direction θ. A polar coordinate plot depicts the variation of $D_{xx}(\theta)$ with θ (Fig. 2*B*).

Comparison of Line and Spot FPR. The accuracy of spot and line FPR measurements of lateral diffusion depends in part on the value of the ratio τ_{xx}/τ_{yy}. Fig. 3 depicts the results of a set of theoretical experiments in which either spot FPR (Fig. 3*A*) or line FPR (Fig. 3*B*) was used to measure the lateral diffusion of a fluorescent marker that has orthogonal "fast" and "slow" diffusion axes characterized by recovery times of τ_{xx} and τ_{yy}, respectively. As expected, spot FPR is most accurate when $\tau_{xx} = \tau_{yy}$, whereas line FPR performs best when $\tau_{xx} << \tau_{yy}$. As τ_{yy} becomes much greater than τ_{xx}, spot FPR measures an average value of τ_{xx} and τ_{yy} that is heavily weighted toward τ_{xx}. A low ratio of τ_{xx}/τ_{yy} is clearly desirable for line FPR measurements. In practice, a low ratio is

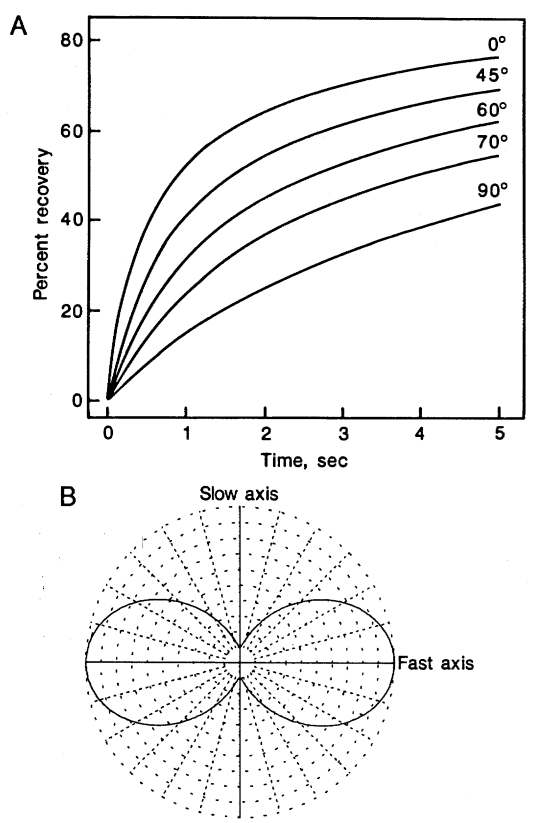

FIG. 2. Effect of sample rotation on recovery kinetics. (*A*) Eq. **6a** was evaluated for $K = 2$, $w_x = 1$ μm, $w_y = 10$ μm, $D_{xx} = 10^{-8}$ cm$^2\cdot$sec^{-1}, $D_{yy} = 10^{-9}$ cm$^2\cdot$sec^{-1}, and $D_{xy} = D_{yx} = 0$ at rotation angles between 0° and 90°. The sample was "rotated" by transforming **D** according to Eq. **11**. The angle between the major axis of the beam and the y axis is indicated above each recovery curve. The ordinate is as described in Fig. 1. The abscissa represents time after photobleaching. (*B*) Effective diffusion rate in the direction θ, $D_{xx}(\theta)$, was calculated from Eq. **12** for $D_{xx} = 10D_{yy}$ and plotted in polar coordinates. The radial coordinate is the diffusion coefficient $D_{xx}(\theta)$; the angular coordinate is the rotation angle. The "fast" axis is horizontal, and the "slow" axis is vertical.

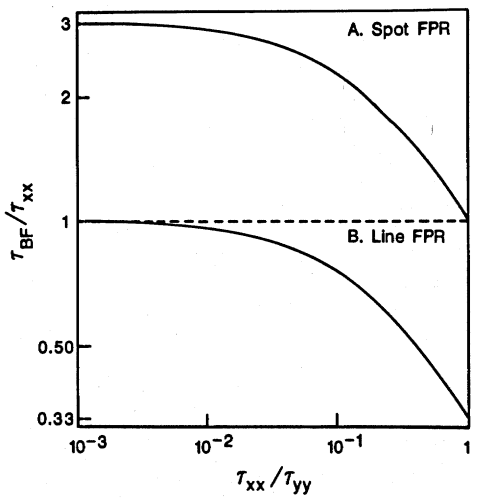

FIG. 3. Effect of τ_{xx}/τ_{yy} ratio on the accuracy of spot and line FPR measurements. Theoretical fluorescence recovery data were best-fit to Eq. 6c (spot FPR, *A*) or Eq. 6b (line FPR, *B*) by the following algorithm. First, $\tau_{1/2}$ for the theoretical data (denoted τ') was determined from Eq. 6a for $K = 2$, $F(\infty) = 1000$, $\tau_{xx} = 1$, and τ_{yy} as indicated. Next, τ_{xx} (from Eq. 6b) or τ (from Eq. 6c) was adjusted so that fluorescence recovery was 50% complete at $t = \tau'$. The resulting best-fit (BF) values (τ_{BF}) for τ (spot FPR) and τ_{xx} (line FPR) are shown in a log–log plot of τ_{BF}/τ_{xx} versus τ_{xx}/τ_{yy}.

achieved by increasing the eccentricity of the elliptical beam (see Eqs. 7a and b).

Experimental Results. Rhodamine-labeled phalloidin was used to stain filamentous actin in IFN-γ-treated HDF (Fig. 4*A*) and HEC (Fig. 4*B*). Prominent actin SF arranged in longitudinal, parallel bundles were observed in both cell types. Phase-contrast microscopy showed that both cell types were markedly elongated (data not shown).

Line FPR was used to measure the lateral diffusion of class I MHC proteins on IFN-γ-treated HEC and HDF. Class I MHC proteins labeled with either W6/32 or anti-β_2m diffused anisotropically on HDF but isotropically on HEC (Table 1). $D_\perp/D_\parallel$, the diffusion anisotropy ratio, was 0.69 and 0.71 for proteins on HDF labeled with anti-β_2m and W6/32, respectively. For both labels, diffusion parallel to the underlying actin SF was faster than diffusion perpendicular to the SF.

The lateral mobility of Flu-PtdEtn on HEC and HDF was measured by line FPR. As shown in Table 2, Flu-PtdEtn diffused isotropically on HEC and on two different strains of HDF. The absence of lipid diffusion anisotropy suggests that neither the elongated cell shape nor plasma membrane corrugations are responsible for anisotropic diffusion of class I MHC proteins on HDF.

Spot FPR was also used to measure the lateral mobility of class I MHC proteins and Flu-PtdEtn on HEC and HDF. Spot and line FPR methods yielded comparable absolute diffusion rates for both protein and lipid (Tables 1 and 2).

DISCUSSION

The experiments reported here were designed to test the hypothesis that anisotropic arrangements of actin SF in IFN-γ-treated HEC would cause transmembrane proteins to diffuse anisotropically (9, 14, 15). Although we found that the diffusion of class I MHC proteins on IFN-γ-treated HDF is anisotropic, our measurements on IFN-γ-treated HEC were not consistent with this hypothesis. Specifically, both class I MHC proteins and a membrane lipid analogue were found to diffuse isotropically in IFN-γ-treated HEC membranes, despite anisotropic cell shape and actin SF organization in this cell type. In light of this negative result, we think it unlikely

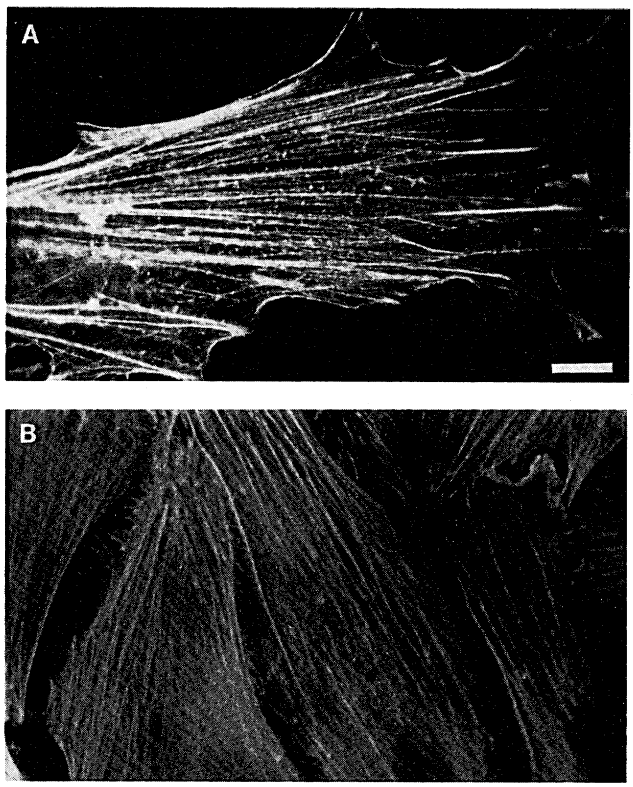

FIG. 4 Fluorescence photomicrographs of rhodamine-labeled phalloidin-stained actin filaments. HDF (*A*) or HEC (*B*) cultures were treated for 4 days with IFN-γ at 200 units/ml and then fixed, permeabilized, and stained with rhodamine-labeled phalloidin (Molecular Probes, Eugene, OR; ref. 2). The actin in both cell types is arranged in longitudinal parallel bundles of stress fibers. Whereas IFN-γ treatment induced changes in HEC shape and SF organization, treatment with this mediator did not affect HDF shape or SF organization (data not shown). (Bar = 10 μm.)

that actin SF are the principal structures restricting HEC membrane protein mobility. The absence of diffusion anisotropy on HEC does not imply a lack of regulation of protein mobility, because class I MHC protein diffusion is significantly slower than that of membrane lipid on this cell type

Table 1. Lateral mobility of class I MHC proteins on HEC and HDF

Cell	Fluorescent antibody	Axis*	$D^\dagger$	$n^\ddagger$	$P^\S$
HEC	Anti-β_2m	⊥	1.8 ± 0.7	5	NS
		∥	1.4 ± 0.8	3	
	W6/32	⊥	1.8 ± 0.6	12	NS
		∥	1.6 ± 0.6	12	
	W6/32	Spot	2.3 ± 0.6	12	
HDF	Anti-β_2m	⊥	1.3 ± 0.4	6	<0.02
		∥	1.9 ± 0.3	6	
	W6/32	⊥	0.7 ± 0.2	7	<0.05
		∥	1.0 ± 0.3	8	
	W6/32	Spot	1.2 ± 0.3	6	

HEC and HDF were treated with IFN-γ at 200 units/ml for 3–5 days. Mobile fractions were >87% for all samples examined.

*Axis refers to the direction of diffusion relative to the orientation of actin SF; ∥ is parallel; ⊥ is perpendicular; spot is a measurement performed with spot FPR.

†*D*, diffusion coefficient (× 10^9 $cm^2 \cdot sec^{-1}$). Values reported are mean ± SD.

‡n, Number of measurements.

§*P*, significance level from two-tailed Student's *t* test; NS, not significant ($P > 0.20$).

Table 2. Lateral mobility of Flu-PtdEtn on HEC and HDF

Cell	Axis	D	n	P
HEC	⊥	8.2 ± 2.0	5	NS
	∥	7.1 ± 2.2	6	
	Spot	8.1 ± 0.8	10	
HDF strain 1	⊥	6.6 ± 1.8	6	NS
	∥	5.7 ± 1.5	7	
HDF strain 2	⊥	5.8 ± 0.6	7	NS
	∥	6.2 ± 1.5	7	
	Spot	5.1 ± 0.5	11	

HEC and HDF were treated with IFN-γ at 200 units/ml for 4 days. Mobile fractions were >97% for all samples examined. Axis, D, n, and P are as described in Table 1.

(Table 2). Cellular structures other than actin SF, such as the "membrane skeleton" (reviewed in ref. 27) or the extracellular matrix, may regulate transmembrane protein mobility and determine diffusion anisotropy.

Anisotropy of membrane protein diffusion has been examined by others. By using the "checkerboard FPR" technique to quantify diffusion anistropy, Smith *et al.* (14) reported diffusion rates of 1.6–14 × 10^{-12} $cm^2 \cdot sec^{-1}$ and mobile fractions of 90–100% for con A receptors on murine fibroblasts. By using the "video-FRAP" technique, Kapitza *et al.* (15) observed diffusion rates of 1–50 × 10^{-11} $cm^2 \cdot sec^{-1}$ and mobile fractions of 20–60% for con A receptors on human foreskin fibroblasts. These diffusion rates and mobile fractions are significantly less than those observed here for class I MHC proteins on IFN-γ-treated HDF and HEC. Furthermore, the con A receptors in the study of Smith *et al.* (14) exhibited marked diffusion anisotropy [$0.1 < (D_\perp/D_\parallel) < 0.5$], whereas the minimum anisotropy ratio observed for class I MHC proteins was 0.69. These differences may reflect differences in the cell type, in the particular family of cell surface molecules detected by the fluorescent probes, or in anchorage modulation of the actin cytoskeleton induced by either succinyl-con A- or residual tetravalent con A-mediated receptor crosslinking (7, 10, 13).

In addition to the biological implications of our work, we have described a theory and method for line FPR. Our data show that diffusion coefficients derived from line and spot FPR measurements are comparable. Moreover, the diffusion rates observed by line FPR for class I MHC proteins on IFN-γ-treated HDF and HEC are similar to values reported for class I MHC protein diffusion on embryonic HDF (28), human neutrophils (29), and virally transformed B cells (30).

The line FPR technique offers several advantages over other FPR methods for detecting and quantifying anisotropic diffusion. Compared to the method of Smith *et al.* (14), line FPR offers faster data acquisition and analysis, higher spatial resolution, lower fluorescence signal requirement, and more accurate determination of diffusion rates. Increased resolution becomes critically important when FPR measurements are performed on small or irregularly shaped cells (31), since photobleaching of a large fraction of the cell surface may produce artifactual slowing of the diffusion rate. Further, line FPR permits diffusion anisotropy to be measured locally on a cell surface, whereas techniques requiring a larger photobleaching geometry detect only global anisotropy. The "scanning line" (18) and video-FRAP (15) methods should offer experimental speed and spatial resolution that are comparable to that of line FPR, although video-FRAP may require a larger fluorescence signal. Although each of these FPR methods is sensitive to diffusion anisotropy on a scale comparable to the characteristic distance for that method, these methods may all fail to detect anisotropy on a much larger or smaller scale.

Membrane nonplanarity may mimic diffusion anisotropy, since FPR methods measure only those molecular motions orthogonal to the laser beam (32). The diffusion tensor can be used to model diffusion on nonplanar surfaces. As a membrane becomes increasingly corrugated in one dimension, the apparent isotropic diffusion rate decreases by a factor of 3 (see Fig. 3*A*). Plasma membrane corrugations in one dimension were not, however, responsible for the diffusion anisotropy of class I MHC proteins on HDF, since Flu-PtdEtn diffused isotropically on this cell type.

In summary, we have devised and applied a method for quantifying anisotropic lateral mobility in cell membranes. We have demonstrated that differences in the mobility of class I MHC proteins on IFN-γ-treated HEC and HDF, two human cell types exhibiting elongated shape and anisotropic SF organization, become apparent only when diffusion anisotropy is examined. Line FPR provides an important tool for the analysis of factors controlling the mobility of membrane constituents.

We thank Patricia Riendeau and Kay Case for cell culture, Yung J. Han for technical assistance, and Bo E. H. Saxberg for helpful discussions. This work was supported by Grants HL 32854 and HL 36003 from the National Institutes of Health. A.H.S. is a fellow of the Medical Scientist Training Program (GM 07753), J.S.P. is an Established Investigator of the American Heart Association, and D.E.G. is a Fellow of The Medical Foundation, Boston, MA.

1. Pober, J. S., Collins, T., Gimbrone, M. A., Jr., Cotran, R. S., Gitlin, J. D., Fiers, W., Clayberger, C., Krensky, A. M., Burakoff, S. J. & Reiss, C. S. (1983) *Nature (London)* **305**, 726–729.
2. Stolpen, A. H., Guinan, E. C., Fiers, W. & Pober, J. S. (1986) *Am. J. Pathol.* **123**, 16–24.
3. Schlessinger, J., Axelrod, D., Koppel, D. E., Webb, W. W. & Elson, E. L. (1977) *Science* **195**, 307–309.
4. Cherry, R. J. (1979) *Biochim. Biophys. Acta* **559**, 289–327.
5. Jacobson, K., O'Dell, D. & August, J. T. (1984) *J. Cell Biol.* **99**, 1624–1633.
6. Nicolson, G. L. (1976) *Biochim. Biophys. Acta* **457**, 57–108.
7. Schlessinger, J., Elson, E. L., Webb, W. W., Yahara, I., Rutishauser, U. & Edelman, G. M. (1977) *Proc. Natl. Acad. Sci. USA* **74**, 1110–1114.
8. Bourguignon, L. Y. W. & Singer, S. J. (1977) *Proc. Natl. Acad. Sci. USA* **74**, 5031–5035.
9. Ash, J. F., Louvard, D. & Singer, S. J. (1977) *Proc. Natl. Acad. Sci. USA* **74**, 5584–5588.
10. Henis, Y. I. & Elson, E. L. (1981) *Proc. Natl. Acad. Sci. USA* **78**, 1072–1076.
11. Pober, J. S., Guild, B. C., Strominger, J. L. & Veatch, W. R. (1981) *Biochemistry* **20**, 5625–5633.
12. Wu, E.-S., Tank, D. W. & Webb, W. W. (1982) *Proc. Natl. Acad. Sci. USA* **79**, 4962–4966.
13. Gall, W. E. & Edelman, G.M. (1981) *Science* **213**, 903–905.
14. Smith, B. A., Clark, W. R. & McConnell, H. M. (1979) *Proc. Natl. Acad. Sci. USA* **76**, 5641–5644.
15. Kapitza, H. G., McGregor, G. & Jacobson, K. A. (1985) *Proc. Natl. Acad. Sci. USA* **82**, 4122–4126.
16. Axelrod, D., Koppel, D. E., Schlessinger, J., Elson, E. & Webb, W. W. (1976) *Biophys. J.* **16**, 1055–1069.
17. Yguerabide, J., Schmidt, J. A. & Yguerabide, E. (1982) *Biophys. J.* **39**, 69–75.
18. Koppel, D. E. (1979) *Biophys. J.* **28**, 281–292.
19. Owicki, J. C. & McConnell, H. M. (1980) *Biophys. J.* **30**, 383–398.
20. Gimbrone, M. A., Jr. (1976) *Prog. Hemostasis Thromb.* **3**, 1–28.
21. Thornton, S. C., Mueller, S. N. & Levine, E. M. (1983) *Science* **222**, 623–625.
22. Scahill, S. J., Devos, R., Van der Heyden, J. & Fiers, W. (1983) *Proc. Natl. Acad. Sci. USA* **80**, 4654–4658.
23. Barnstable, C. J., Bodmer, W. F., Brown, G., Galfre, G., Milstein, C., Williams, A. F. & Ziegler, A. (1978) *Cell* **14**, 9–20.
24. Goding, J. W. (1976) *J. Immunol. Methods* **13**, 215–226.
25. Golan, D. E., Brown, C. S., Cianci, C. M. L., Furlong, S. T. & Caulfield, J. P. (1986) *J. Cell Biol.* **103**, 819–828.
26. Bevington, P. R. (1969) *Data Reduction and Error Analysis for the Physical Sciences* (McGraw-Hill, New York).
27. Marchesi, V. T. (1985) *Annu. Rev. Cell Biol.* **1**, 531–561.
28. Wier, M. L. & Edidin, M. (1986) *J. Cell Biol.* **103**, 215–222.
29. Petty, H. R., Smith, L. M., Fearon, D. T. & McConnell, H. M. (1980) *Proc. Natl. Acad. Sci. USA* **77**, 6587–6591.
30. Bierer, B. E., Herrmann, S. H., Brown, C. S., Burakoff, S. J. & Golan, D. E. (1987) *J. Cell Biol.* **105**, 1147–1152.
31. Wolf, D. E., Hagopian, S. S., Lewis, R. G., Voglmayr, J. K. & Fairbanks, G. (1986) *J. Cell Biol.* **102**, 1826–1831.
32. Aizenbud, B. M. & Gershon, N. D. (1985) *Biophys. J.* **48**, 543–546.